Deletion of a Long-Range *Dlx5* Enhancer Disrupts Inner Ear Development in Mice

Kenneth R. Johnson,*,[1] Leona H. Gagnon,* Cong Tian,*,[†] Chantal M. Longo-Guess,* Benjamin E. Low,[‡] Michael V. Wiles,[‡] and Amy E. Kiernan[§,]**

*The Jackson Laboratory, Bar Harbor, Maine 04609, [†]Graduate School of Biomedical Sciences and Engineering, University of Maine, Orono, Maine 04469, [‡]Technology Evaluation and Development, The Jackson Laboratory, Bar Harbor, Maine 04609, [§]Department of Ophthalmology, and **Department of Genetics, University of Rochester, New York 14642

ORCID ID: 0000-0002-0448-2604 (K.R.J.)

ABSTRACT Distal enhancers are thought to play important roles in the spatiotemporal regulation of gene expression during embryonic development, but few predicted enhancer elements have been shown to affect transcription of their endogenous genes or to alter phenotypes when disrupted. Here, we demonstrate that a 123.6-kb deletion within the mouse *Slc25a13* gene is associated with reduced transcription of *Dlx5*, a gene located 660 kb away. Mice homozygous for the *Slc25a13* deletion mutation [named hyperspin (*hspn*)] have malformed inner ears and are deaf with balance defects, whereas previously reported *Slc25a13* knockout mice showed no phenotypic abnormalities. Inner ears of $Slc25a13^{hspn/hspn}$ mice have malformations similar to those of $Dlx5^{-/-}$ embryos, and *Dlx5* expression is severely reduced in the otocyst but not the branchial arches of $Slc25a13^{hspn/hspn}$ embryos, indicating that the $Slc25a13^{hspn}$ deletion affects otic-specific enhancers of *Dlx5*. In addition, transheterozygous $Slc25a13^{+/hspn}$ $Dlx5^{+/-}$ mice exhibit noncomplementation with inner ear dysmorphologies similar to those of $Slc25a13^{hspn/hspn}$ and $Dlx5^{-/-}$embryos, verifying a *cis*-acting effect of the $Slc25a13^{hspn}$ deletion on *Dlx5* expression. CRISPR/Cas9-mediated deletions of putative enhancer elements located within the $Slc25a13^{hspn}$ deleted region failed to phenocopy the defects of $Slc25a13^{hspn/hspn}$ mice, suggesting the possibility of multiple enhancers with redundant functions. Our findings in mice suggest that analogous enhancer elements in the human *SLC25A13* gene may regulate *DLX5* expression and underlie the hearing loss that is associated with split-hand/-foot malformation 1 syndrome. $Slc25a13^{hspn/hspn}$ mice provide a new animal model for studying long-range enhancer effects on *Dlx5* expression in the developing inner ear.

KEYWORDS *Dlx5*; *Slc25a13*; SHFM1; inner ear; distal enhancer

RECENT genome-wide studies of chromatin and transcription factor signatures have revealed the prevalence of *cis*-regulatory elements (enhancers) in the genome and their potential importance in determining spatial, temporal, and quantitative patterns of gene expression (Visel *et al.* 2009; Bulger and Groudine 2011; Daniel *et al.* 2014; Shlyueva *et al.* 2014; Coppola *et al.* 2016). Classical gene-centric studies, which rely on phenotypic consequences to identify enhancer function, have identified only a few human diseases that are caused by enhancer disruptions, and these usually involve dysregulation of key developmental control genes (Kleinjan and van Heyningen 2005). The distal-less homeobox proteins DLX5 and DLX6 are developmentally important transcription factors thought to be regulated by multiple tissue-specific enhancers (Birnbaum *et al.* 2012), and deletions or disruptions of these enhancers are thought to contribute to the various anomalies associated with split-hand/-foot malformation 1 (SHFM1) (Rasmussen *et al.* 2016), the SHFM syndrome mapped to chromosome 7q21 [Online Mendelian Inheritance in Man (OMIM) 220600].

Clinical features of the SHFM1 locus sometimes include craniofacial anomalies and hearing loss as well as the characteristic limb malformation (Ignatius *et al.* 1996; Haberlandt *et al.* 2001; Tackels-Horne *et al.* 2001; Wieland *et al.* 2004; Bernardini *et al.* 2008; Saitsu *et al.* 2009). Linkage mapping and analysis of cytogenetic abnormalities have defined the SHFM1 chromosomal region to a ~1.5-Mb interval that

doi: https://doi.org/10.1534/genetics.117.300447
Manuscript received October 30, 2017; accepted for publication December 9, 2017; published Early Online January 3, 2018.
Supplemental material is available online at www.genetics.org/lookup/suppl/doi:10.1534/genetics.117.300447/-/DC1.
[1]Corresponding author: The Jackson Laboratory, 600 Main St., Bar Harbor, ME 04609. E-mail: ken.johnson@jax.org

includes five known genes: *DYNC1I1*, *SLC25A13*, *SEM1*, *DLX5*, and *DLX6* (Scherer *et al.* 1994; Marinoni *et al.* 1995; Haberlandt *et al.* 2001; Tackels-Horne *et al.* 2001; Wieland *et al.* 2004; van Silfhout *et al.* 2009; Brown *et al.* 2010; Birnbaum *et al.* 2012). *DLX5* and *DLX6* are considered the primary candidate genes for SHFM1 because of their role in appendicular skeletal development (Robledo *et al.* 2002), and because mice with double mutations of these genes exhibit bilateral limb defects typical of SHFM1 (Merlo *et al.* 2002a; Robledo *et al.* 2002; Robledo and Lufkin 2006). *DLX5* intragenic mutations have been found in a few SHFM1 patients, supporting an underlying role for this gene in the SHFM1 limb malformation (Shamseldin *et al.* 2012; Sowinska-Seidler *et al.* 2014; Wang *et al.* 2014) and in the hearing loss associated with SHFM1D (Shamseldin *et al.* 2012). Most cases of SHFM1, however, are associated with chromosomal aberrations—including deletions, inversions, and translocations—that do not directly include *DLX5* or *DLX6* (Birnbaum *et al.* 2012; Rasmussen *et al.* 2016). Disruptions of tissue-specific, long-range enhancers that regulate *DLX5/DLX6* expression are thought to underlie most cases of SHFM1 (Birnbaum *et al.* 2012). Although predicted enhancer elements for SHFM1-associated phenotypes were shown to enhance transcription of reporter genes in transgenic zebrafish and mice, their effects on endogenous *Dlx5* or *Dlx6* expression and the phenotypic consequences of their loss have not been determined.

Though most studies have focused on *DLX5* and *DLX6* dysfunction or dysregulation as the primary causes for SHFM1, indirect evidence from tissue expression patterns suggests that other genes in the region may also contribute to the phenotype. For example, the solute carrier family 25 member 13 gene (*SLC25A13*) lies within the 1.2-Mb SHFM1 minimal critical region, and the orthologous gene in mice (*Slc25a13*) is expressed in limb buds, branchial arches, and otic vesicle (Sinasac *et al.* 1999; del Arco *et al.* 2002; Birnbaum *et al.* 2012); suggesting a possible role for this gene in development of the limb, craniofacial, and inner ear anomalies of the SHFM1 phenotype. Mice with targeted and gene trap mutations of *Slc25a13* (Sinasac *et al.* 2004; Contreras *et al.* 2007), however, have normal limb morphology. Likewise, human mutations of *SLC25A13*, although they underlie cases of citrullinemia (CTLN2; OMIM 603471) and neonatal intrahepatic cholestasis (NICCD; OMIM 605814), do not result in SHFM1-like abnormalities or hearing loss (Saheki and Kobayashi 2002).

Here, we report on the discovery and characterization of a new, naturally occurring, recessive mouse mutation named hyperspin (*hspn*) and show that it is a 123.6-kb deletion within the *Slc25a13* gene. Most homozygous mutant mice ($Slc25a13^{hspn/hspn}$) are viable and fertile; however, in contrast to the normal phenotype of previously reported *Slc25a13* mutations (Sinasac *et al.* 2004; Contreras *et al.* 2007), they exhibit rapid circling and head-shaking behaviors typical of vestibular dysfunction and they are deaf with malformed inner ears. Because of the similarities in the inner ear dysmorphologies of $Slc25a13^{hspn/hspn}$ and *Dlx5* knockout mice (Acampora *et al.* 1999; Depew *et al.* 1999; Merlo *et al.* 2002b), we hypothesized and provide evidence that the loss of long-range *cis*-regulatory elements located within the $Slc25a13^{hspn}$ deletion causes a reduction in *Dlx5* expression during inner ear development. The mammalian inner ear is a very complex and intricate structure that requires a highly orchestrated pattern of cell-type and stage-specific transcriptional regulation for its development. Our discovery of distal-acting, *cis*-regulatory elements that specifically enhance *Dlx5* expression in the otocyst of mouse embryos adds to our understanding of how such precise patterning of gene expression is achieved.

Materials and Methods

Mouse husbandry

All mice in this study were obtained from research or production colonies and housed in the Research Animal Facility at The Jackson Laboratory (JAX) in Bar Harbor, ME. JAX is accredited by the American Association for the Accreditation of Laboratory Animal Care. All procedures involving the use of mice were approved by the JAX Institutional Animal Care and Use Committee and were performed in accordance with the guidelines and regulations of the US National Institutes of Health Office of Laboratory Animal Welfare and the Public Health Service Policy on the Humane Care and Use of Laboratory Animals.

Embryonic stages of mice were determined from timed matings by observing females for vaginal plugs. The day of the plug was considered embryonic day 0.5 (E0.5).

The hspn mutation of Slc25a13

The recessive *hspn* mutation arose spontaneously in the CXJ1/SalkJ recombinant inbred strain, and was shown to have occurred on the SJL/J-derived strand of DNA, as determined by markers that are polymorphic between BALB/c and SJL/J. Mutant mice (*hspn/hspn*) are identified by their hyperactive circling behavior. To alleviate the severe skin lesions that occurred in mutant mice of the CXJ1/SalkJ-*hspn* strain, a congenic inbred strain was developed by repeated backcrossing of mutant mice to the C57BL/6J inbred strain until achieving the equivalent of 10 backcross generations, followed by inbreeding to generate the B6.SJL(C)-$Slc25a13^{hspn}$/Kjn congenic strain which is available from JAX as stock #5679. All studies described here were done with mice of the B6.SJL(C)-$Slc25a13^{hspn}$/Kjn congenic strain.

Development of Slc25a13 knockout mice

A knockout allele of the *Slc25a13* gene was produced using a combination of recombineering (Liu *et al.* 2003; Warming *et al.* 2005) and standard molecular cloning techniques. As diagramed in Supplemental Material, Figure S1, a 10,696-bp fragment of the *Slc25a13* gene containing the targeted exon 5 was retrieved from a bacterial artificial chromosome and cloned into a targeting vector. Exon 5 (140 bp) was chosen for targeting because it is present in all known protein-coding

transcripts of the gene and its deletion would cause an early disruption of the reading frame. A PGK-Neo selection cassette was then integrated into the targeting vector by homologous recombination. After electroporation of the targeting vector into C57BL/6N JM8A3 embryonic stem (ES) cells, ES cells with the targeted mutant allele were identified by G418 selection and confirmed by Southern blot and loss-of-allele assays. Verified ES cells were then microinjected into C57BL/6NJ host blastocysts. Progeny from host females were selected for the presence of PGK-Neo and the mutant *Slc25a13* allele and used to establish a homozygous C57BL/6J-*Slc25a13*^{tm2Kjn}/Kjn knockout line. The floxed PGK-Neo cassette was removed from this line by mating with mice of the B6.Cg-Tg(Sox2-cre)1Amc/J strain (stock #8454; JAX). The resulting progeny from this cross, which were heterozygous for the *Slc25a13* knockout allele but lacking the PGK-Neo cassette and the Cre transgene, were intercrossed to establish the homozygous knockout line STOCK-*Slc25a13*$^{tm2.1Kjn}$/Kjn (stock #29351; JAX), which was used for the studies described here.

Auditory-evoked brain stem response

Hearing in mice was assessed by auditory-evoked brain stem response (ABR) threshold analysis. Mice were anesthetized with an intraperitoneal injection of tribromoethanol (0.2 ml of 20 mg/ml stock per 10 g of body weight), and then placed on a 37° temperature-controlled pad in a sound-attenuating chamber. Needle electrodes were placed just under the skin, with the active electrode placed between the ears just above the vertex of the skull, the ground electrode between the eyes, and the reference electrode underneath the left ear. High-frequency transducers were placed just inside the ear canal and computer-generated sound stimuli were presented at defined intervals. Thresholds were determined for broadband clicks and 8-, 16-, and 32-kHz pure-tone stimuli by increasing the sound pressure level (SPL) in 10-dB increments followed by 5-dB increases and decreases to determine the lowest level at which a distinct ABR wave pattern could be recognized. Stimulus presentation and data acquisition were performed using the Smart EP Evoked Potential System (Intelligent Hearing Systems, Miami, FL).

Scanning electron microscopy

For scanning electron microscopy (SEM) analysis, inner ears were dissected and fixed in 2.5% glutaraldehyde in 0.1 M cacodylate buffer for 4 hr at 4°, and then subjected to two 10 min washes in 0.1 M phosphate buffer. The cochlear shell and the stria vascularis were dissected away to expose the organ of Corti, and the sample was then postfixed with 1% osmium tetroxide in 0.1 M phosphate buffer, treated with thiocarbohydrazide, dehydrated, and critical-point dried (Self *et al.* 1998). After mounting, samples were sputter coated to produce a 15-nm gold/palladium coating and examined at 20 kV (Z = 15) on a Hitachi (Tokyo, Japan) S-3000 Scanning Electron Microscope. Images were processed and preserved using Quartz.PCI (version 5.1) software (Quartz, Vancouver, Canada).

Adult inner ear whole-mount preparations

Whole-mount preparations of adult inner ears were used to examine otoconia and gross morphology. Inner ears were dissected and flushed with neutral-buffered formalin (NBF) through a hole at the cochlear apex. Inner ears were then immersed in NBF, rinsed with distilled deionized water, and then dehydrated by 2-hr immersions in 70% ethanol, 95% ethanol, and two dehydration rounds in 100% ethanol, and then dried well. Inner ears were then cleared and stored in methyl salicylate. Inner ear whole mounts were viewed using polarized light on a Leica MZ 12_5 dissecting microscope, and images were captured and archived using the Leica DFC 425 camera and Leica Application Suite version 3.6.0 (Leica Microsystems, Wetzlar, Germany).

Inner ear paintfills

Paintfill analysis of embryonic inner ears was adapted and performed as previously described (Kiernan 2006). Briefly, embryonic mice (E15.5) were decapitated and the heads bisected and fixed overnight in Bodian's fixative. Heads were then dehydrated in ethanol serial washes, and cleared overnight in methyl salicylate. Several microliters of paint suspension (1% white gloss latex paint or white-out correction fluid in methyl salicylate) were injected into the middle turn of the cochlea. The paintfilled inner ear was then dissected away from the rest of the head.

Whole-mount RNA in situ hybridization

Dlx5 expression in whole-mount embryos was examined by *in situ* hybridization. RNA from newborn mouse inner ears was reversely transcribed with the iScript cDNA Synthesis Kit (1708890; Bio-Rad, Hercules, CA), and a template complementary DNA for SP6 transcription was amplified using PCR primers DLX5F (5′-CAGGTGAAAATCTGGTTTCAGAAC-3′) and Sp6-DLX5R (5′-GCGATTTAGGTGACACTATAGGCACCATTGATAGTGTCCACAGTTG-3′) and used to produce a digoxigenin (DIG)-labeled RNA probe (11175025910; Roche). Embryos from timed matings were collected at E9.5 and E10.5 and genotyped by PCR of tail-tip DNA. RNA *in situ* hybridization was performed according to previously described methods (Piette *et al.* 2008). Homozygous *hspn* and wild-type embryos were transferred to clean vials containing 4% paraformaldehyde (PFA) in PBS, the solution was refreshed, and fixation continued at 4° overnight while gently rocking. The following day, embryos were dehydrated through a series of methanol washes and stored in 100% methanol. Embryos were rehydrated using methanol/PBS with Tween 20 (PBST) washes and incubated for 9.5 min in 10 μg/ml proteinase K, rinsed, and refixed in 4% PFA/0.2% glutaraldehyde in PBST. Embryos were washed in 50% hybridization solution/50% PBST for 3 min, in 100% hybridization solution for 3 min, and then prehybridized for 3 hr in fresh 100% hybridization solution at 65°. Denatured DIG-labeled riboprobe was then added to the embryos and hybridized overnight at 70° while rocking. The next day, the embryos were washed and incubated with 1 ml of antibody buffer for 2 hr while rocking. After the

antibody buffer was removed, preblocked anti-DIG antibody was added and incubated at 4° overnight. The next day, embryos were washed and incubated in 1 ml of BM Purple (11442074001; Sigma-Aldrich, St. Louis, MO) covered in foil while rocking overnight. When sufficient staining was achieved, embryos were washed with stop solution followed by methanol dehydration. Whole embryos were transferred to a small petri dish and imaged under an inverted light microscope.

Genetic mapping and genotyping of the hspn mutation

Genomic DNA for mapping and genotyping was prepared from tail tips by the HotSHOT procedure (Truett *et al.* 2000). PCR reactions were performed using the 5 PRIME MasterTaq Kit (catalog number 2200210) in accordance with the manufacturer's instructions, and run in a Bio-Rad Peltier Thermal Cycler. Amplification consisted of one cycle of denaturation at 97° for 30 sec followed by 40 cycles, each consisting of 94° for 30 sec, 58° for 30 sec, and 72° for 30 plus 1 sec per cycle. After the 40 cycles, the final product was extended for 10 min at 72°. PCR products were visualized on 3% NuSieve (Lonza Bioscience, Rockland, ME) agarose gels.

To genetically map the *hspn* mutation, female mice from the B6.SJL(c)-*Slc25a13*^{hspn}/Kjn congenic strain were mated to CAST/EiJ males. The resulting F_1 hybrid progeny (+/*hspn*) were intercrossed and F_2 mice were analyzed for linkage analysis with genetic markers on all chromosomes. Only phenotypically mutant mice recognized by their rapid circling behavior (presumed *hspn/hspn*) were used for the initial *hspn* map location, and remaining F_2 progeny with nonmutant phenotypes were subsequently used for fine mapping. Linkage associations were identified by the concordance between *hspn* genotypes deduced from mouse phenotypes and genotypes of microsatellite DNA markers typed by PCR amplification. Data analysis was performed using the Map Manager QTX (http://www.complextrait.org/archive/2002/html/manly.html) and Microsoft Office Excel (http://office.microsoft.com) software programs.

A three-primer PCR assay was developed to distinguish *hspn* and wild-type alleles. A wild-type-specific forward primer (WT-F, 5′-GGTCGTAGCTCGTGTCTTCC-3′), a *hspn*-specific forward primer (mut-F, 5′-CTCTCTGCAGGTTTCCCTTG-3′), and a common reverse primer (common-R, 5′-CAATGA GAACTGAGTATTAGAGGCTG-3′) were combined in a PCR reaction under conditions as described above. The PCR product size for the PCR product with the *hspn* deletion mutation is 205 bp, and the PCR product size for the wild-type allele is 160 bp.

Candidate gene DNA sequence analysis

PCR reactions for DNA sequencing were performed in the same manner as described above for microsatellite markers in genetic mapping. The PCR primers used to amplify specific regions of each gene evaluated were selected by flanking each evaluated exon using the Primer3 computer program (http://bioinfo.ut.ee/primer3/). PCR products were purified with the QIAquick PCR Purification Kit (QIAGEN, Valencia, CA), sequenced using the Applied Biosystems (Foster City, CA) BigDye Terminator ready reaction kit (version 3.1), and data analysis was performed using Applied Biosystems Sequencing Analysis Software (version 5.2).

Mouse strains with CRISPR/Cas9-mediated deletions

The formal names and JAX stock numbers for the inbred mouse strains with CRISPR/Cas9-generated deletions corresponding to specific regions within the *Slc25a13* gene are shown in Table S1. These strains were used for *in vivo* tests of putative *Dlx5* enhancer effects. To generate the *Slc25A13* deletions, zygotes were collected from naturally mated superovulated female C57BL/6J mice and pronuclear microinjected using ~2–5 pl of 10 mm Tris, 0.5 mM EDTA, pH 7.5 (IDT); a 0.2 unit/μl RNase inhibitor (RNAsin; Promega, Madison, WI) with Cas9 messenger RNA (mRNA) at 100 ng/μl (Trilink Biotechnologies); plus two single guide RNAs (sgRNAs) at 50 ng/μl each, flanking the targeted region, as described previously (Low *et al.* 2016). The 25-kb region deletion also used an oligonucleotide (200-mer, 3 ng/μl IDT) bridging the two cut sites. When possible, truncated sgRNAs were used to reduce the probability of off-target effects (Fu *et al.* 2014). sgRNA targeting regions were designed using the Web-based software packages ZiFiT (http://zifit.partners.org/ZiFiT/), CRISPR Design (http://crispr.mit.edu), and Breaking-Cas (http://bioinfogp.cnb.csic.es/tools/breakingcas/). Microinjected zygotes were transferred to pseudopregnant females and carried to term. At weaning age, genomic DNA from tail tip or ear punches was used to identify founders of interest by PCR amplification with primers spanning the deleted region, followed by Sanger sequencing. Putative founder mice showing deletions of the appropriate size and location were crossed to wild-type C57BL/6J mice to produce N_1 generation mice. After final characterization of the transmitted alleles in N_1 mice, selected individuals were intercrossed to establish homozygous lines. The individual sequences for each target and the PCR primers used to identify the alleles are shown in Table S1.

Data availability

All mouse strains examined in this study are commercially available from JAX. All data necessary for confirming the conclusions presented in the article are represented fully within the article.

Results

The inner ear phenotype of hspn mutant mice

hspn mutant mice (*hspn/hspn*) exhibit rapid circling and head-shaking behavior and are unable to swim. These behaviors indicate inner ear dysfunction, which often includes hearing impairment. We therefore used ABR thresholds to assess the hearing sensitivity of individual *hspn* mutant and control mice (Figure 1A). At 4–5 weeks of age, ABR wave

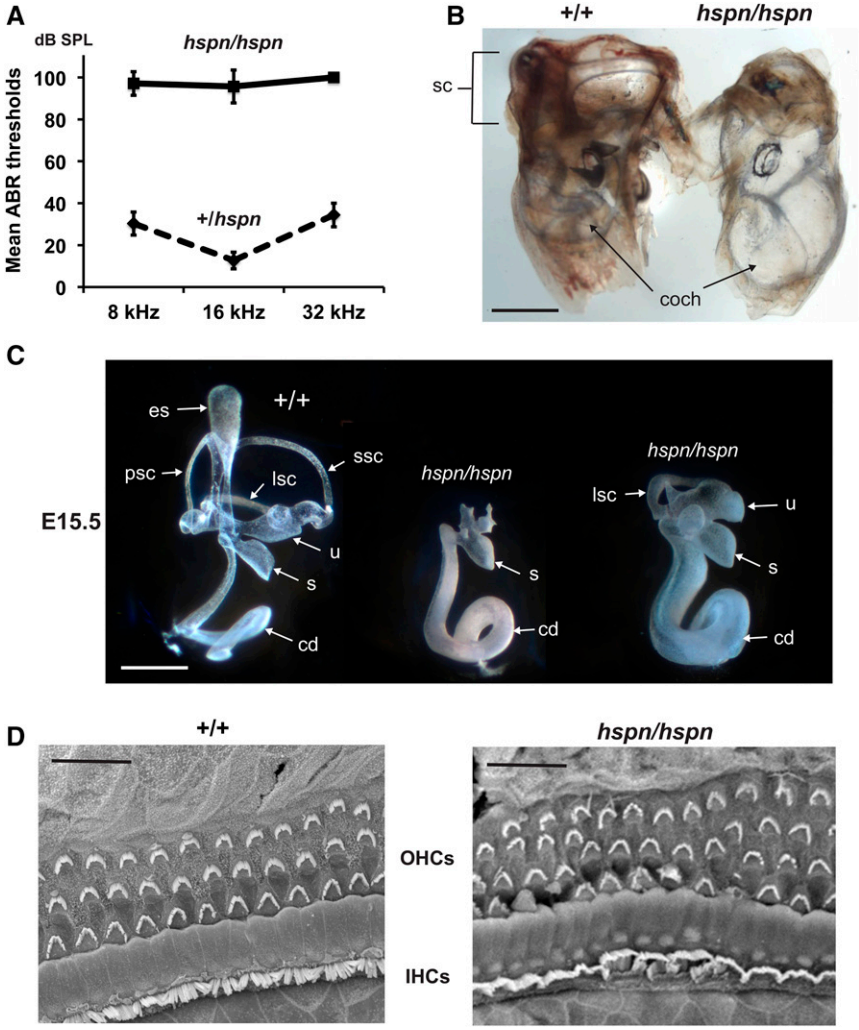

Figure 1 Inner ear phenotype of *hspn/hspn* mutant mice. (A) Hearing assessment by ABR. Average ABR thresholds of *+/hspn* heterozygous control mice ($N = 32$) tested at 5–12 weeks of age compared with those of *hspn/hspn* mutants ($N = 7$) tested at 4–5 weeks of age. The *+/hspn* control mice exhibited normal thresholds at all test frequencies (8, 16, and 32 kHz), whereas the highly elevated ABR thresholds of *hspn/hspn* mutant mice indicated profound hearing impairment. Error bars represent SD. (B) Cleared whole mounts of inner ears from 4-week-old adult mice. Inner ears of the adult *hspn/hspn* mutant shows reduced development of the semicircular canals (sc) and a much wider and shorter cochlea (coch) than that of the +/+ control. Bar, 1 mm. (C) Paintfills of the membranous labyrinths of inner ears from E15.5 embryos. Compared with the normal morphology of +/+ controls, inner ears of *hspn/hspn* mutants lack an endolymphatic sac (es) and duct, have a severe reduction in semicircular canal development, and exhibit a swollen and shortened cochlear duct (cd). The saccule (s) and cochlear duct were present in all *hspn/hspn* mutant inner ears examined; however, the extent of dorsal structure development varied. Posterior semicircular canals (psc) and superior semicircular canals (ssc) never developed in mutant inner ears, but there was variable development of the lateral semicircular canal (lsc) and utricle (u). Bar, 0.5 mm. (D) SEM surface images of the organ of Corti in the midapical region of the cochlea from a 4-week-old *hspn/hspn* mutant mouse and an age-matched +/+ control. Although a single row of inner hair cells (IHCs) and three rows of outer hair cells (OHCs) are present in both mutant and control mice, the hair cells of *hspn/hspn* mutant mice are disorganized, with an extra row of OHCs near the cochlear apex. Bar, 20 μm.

patterns could not be detected for pure-tone 8-, 16-, and 32-kHz stimuli in *hspn/hspn* mutant mice even at the highest sound intensity presented (100-dB SPL), thus demonstrating that these mice are profoundly deaf. Heterozygous mice (*+/hspn*) exhibited normal behavior and swimming ability, and their ABR thresholds at 5–12 weeks of age did not differ from those of littermate wild-type (+/+) mice, confirming the recessive nature of the *hspn* mutation.

Examination of cleared whole-mount preparations of inner ears from adult mice (5 weeks of age) revealed that the inner ears of *hspn* mutant mice are small and malformed compared with those of control mice (Figure 1B). In *hspn* mutants, the cochlea appears abnormally swollen with fewer turns than controls, and all three semicircular canals appear absent, reduced, or malformed. To investigate the observed inner ear malformations in more detail and at an earlier time point, E15.5 embryos were collected for inner ear paintfill analysis (Kiernan 2006). Inner ears of *hspn* mutant embryos displayed variable dysmorphologies, with the most severe defects occurring in the dorsal, vestibular part of the inner ear (Figure 1C). In inner ears of all mutant embryos examined ($N = 7$), the endolymphatic duct and sac and the superior and posterior semicircular canals were missing, and—in all but one—the lateral semicircular canal and utricle were also missing. Although the cochlea is present in all mutant inner ears, the cochlear duct appears to be undercoiled and wider than that of controls.

Because the gross structure of the cochlea of *hspn/hspn* mutants appeared only moderately affected, we investigated potential cellular defects within the cochlear duct, which contains the sensory hair cells. We used SEM to examine organ of Corti surface preparations from six wild-type and four *hspn* mutant mice at 4 weeks of age (Figure 1D). Throughout the basal and middle turns of the *hspn* mutant cochlea, we observed the normal pattern of three rows of outer hair cells and single row of inner hair cells with properly aligned hair bundles, but with occasional missing hair bundles, indicating the onset of hair cell degeneration. However, the apical turn of the cochlea contained an additional fourth and occasional fifth row of outer hair cells and abnormal orientations of hair bundles. The increase in hair-cell rows in the apical region is likely related to the shortened cochlea,

possibly due to incomplete convergent extension (Ma *et al.* 2000; Pauley *et al.* 2006; Kopecky *et al.* 2011). Overall, however, hair-cell formation and the general patterning of the cochlear duct do not appear significantly altered in the *hspn* mutants. The profound deafness of *hspn* mutant mice (Figure 1A) is most likely a consequence of the failure to develop a functional endolymphatic sac (Figure 1C). The endolymphatic sac regulates ion transport and fluid homeostasis in the inner ear. A failure of fluid absorption by the endolymphatic sac would cause dilatation of the membranous labyrinth, as seen in *hspn* mutant embryos (Figure 1C), and result in the increased cochlear diameter observed in adult mutants (Figure 1B). A similar expansion of endolymph volume and ionic imbalance during inner ear development is thought to underlie the deafness exhibited by mice with *Slc26a4* (Kim and Wangemann 2010), *Foxi1* (Hulander *et al.* 2003), *Atp6v0a4* (Lorente-Canovas *et al.* 2013), and *Atp6v1b1* (Tian *et al.* 2017) mutations.

Genetic mapping and molecular characterization of the hspn mutation

hspn mutant mice from the B6.SJL-*Slc25a13* ^{hspn}/Kjn congenic strain were used for all phenotypic and genetic analyses. To genetically map the *hspn* mutation, we analyzed mutant (*hspn/hspn*) F_2 progeny from an intercross of B6.SJL-*Slc25a13* ^{hspn}/Kjn × CAST/EiJ F_1 hybrids. Cosegregation analysis of 211 F_2 mutant (*hspn/hspn*) mice with genetic markers on all chromosomes localized the *hspn* mutation to a 1.2-Mb region on chromosome 6 (Chr 6), between *D6Mit296* (Chr 6: 5.7-Mb position; GRCm38) and *D6Mit139* (Chr 6: 6.9 Mb). The *Dlx5* and *Dlx6* genes are located in this region and were considered good candidates for *hspn* because mice with targeted mutant alleles of *Dlx5*, though they exhibit perinatal lethality, have dysmorphic inner ears similar to what we observed for *hspn/hspn* mice (Depew *et al.* 1999). However, exon sequence analysis of *Dlx5* and its neighbor, *Dlx6*, including splice recognition sequences, revealed no DNA abnormalities and RT-PCR of inner ear mRNA for each of these genes produced amplicons of appropriate size and sequence.

Linkage analysis of 81 additional mutant F_2 mice from the same linkage cross and typing of additional polymorphic CA-repeat markers spanning the 1.2-Mb candidate interval further refined it to a 0.8-Mb region (Chr 6: 5.86–6.66 Mb; GRCm38), which definitively eliminated *Dlx5* and *Dlx6* (Chr 6: 6.87–6.88 Mb) as candidate genes. The refined *hspn* candidate region included part of *Dync1i1* (Chr 6: 5.73–6.22 Mb) and all of *Slc25a13* (Chr 6: 6.04–6.22 Mb) and *Sem1* (Chr 6: 6.56–6.58 Mb). Upon exon sequence analysis of these genes, a large deletion was detected in the *Slc25a13* gene, but no DNA alterations were found in exonic regions of *Dync1i1* or *Sem1*. The presence or absence of small PCR products from multiple locations spanning the genomic region around *Slc25a13* further refined the extent of the deletion. Comparisons of PCR-amplified DNA sequences between wild-type and *hspn/hspn* mice using primers corresponding to sites on either side of the deletion precisely defined the deletion as extending from within intron 3 to exon 17 of *Slc25a13* (Chr 6: 6,042,586- to 6,166,170-bp position; GRCm38), deleting 123.6 kb of genomic DNA (Figure 2A). No additional chromosomal rearrangements were detected in the 0.8-Mb *hspn* candidate region. Most of the 123.6-kb deletion is comprised of noncoding introns but also contains exons 4–17, which encode most of the SLC25A13 protein, including the EF-hand and mitochondrial carrier domains (Figure 2B). A three-primer PCR assay was developed to distinguish *hspn* and wild-type alleles (Figure 2C; *Materials and Methods*).

Generation and phenotype of a targeted Slc25a13 knockout mutation

The protein encoded by *Slc25a13* has a strongly bipartite structure (Figure 2B): the N-terminal domain includes two sets of calcium-binding EF hands, and the C-terminal domain functions as a mitochondrial membrane-bound transporter that participates in the malate aspartate shuttle which supplies aspartate from the mitochondria to the cytosol (Palmieri *et al.* 2001). Human *SLC25A13* mutations perturb the mitochondrial transporter domain of SLC25A13, but do not alter the N-terminal EF-hand domain (Saheki and Kobayashi 2002). The previously reported mouse mutation *Slc25a13*^{tm1Lct} deletes exon 10 and mimics the human mutation 851del4 (Sinasac *et al.* 2004). DNA sequences downstream of exon 10, which encode the C-terminal mitochondrial transporter domain, are eliminated in this mutation; but the upstream region encoding the N-terminal EF-hand domain may still be transcribed. It is possible, therefore, that the *Slc25a13*^{tm1Lct} mutation produces a truncated protein isoform that retains some function during development, which may disrupt inner ear development and be at least partially responsible for the *hspn* mutant phenotype.

To address this possibility and to assess the hearing sensitivity of *Slc25a13* knockout mice (which has not been previously reported), we generated a new knockout mutation of *Slc25a13* with a deletion of exon 5 (Figure S1) which disrupts the reading frame and eliminates both domains of the protein (Figure 2). Mice homozygous for the new knockout mutation (STOCK-*Slc25a13*$^{tm2.1Kjn}$/Kjn)—like previously reported genetically engineered *Slc25a13* mutants—are viable, fertile, and do not exhibit any overt abnormalities. In contrast to *Slc25a13*$^{hspn/hspn}$ mutant mice, the *Slc25a13*$^{tm2.1Kjn}$ knockout mice (*Slc25a13*$^{-/-}$) do not exhibit the circling or head-tossing behaviors characteristic of vestibular dysfunction and they have normal ABR thresholds (Figure S2), indicating normal inner ear function. The severe phenotype of *hspn* mutant mice, therefore, is not caused by loss of protein function, but must rather be due to the loss of regulatory sequences within the noncoding regions of the *Slc25a13* gene.

The mouse Slc25a13^{hspn} deletion in relation to the SHFM1 locus on human chromosome 7

The arrangement of genes within the SHFM1 region of human chromosome 7 (*DYNC1L1*, *SLC25A13*, *SEM1*, *DLX5*, and *DLX6*) corresponds closely with that of the orthologous genes on proximal mouse Chr 6 (Figure 3, A and B). Chromosomal deletions

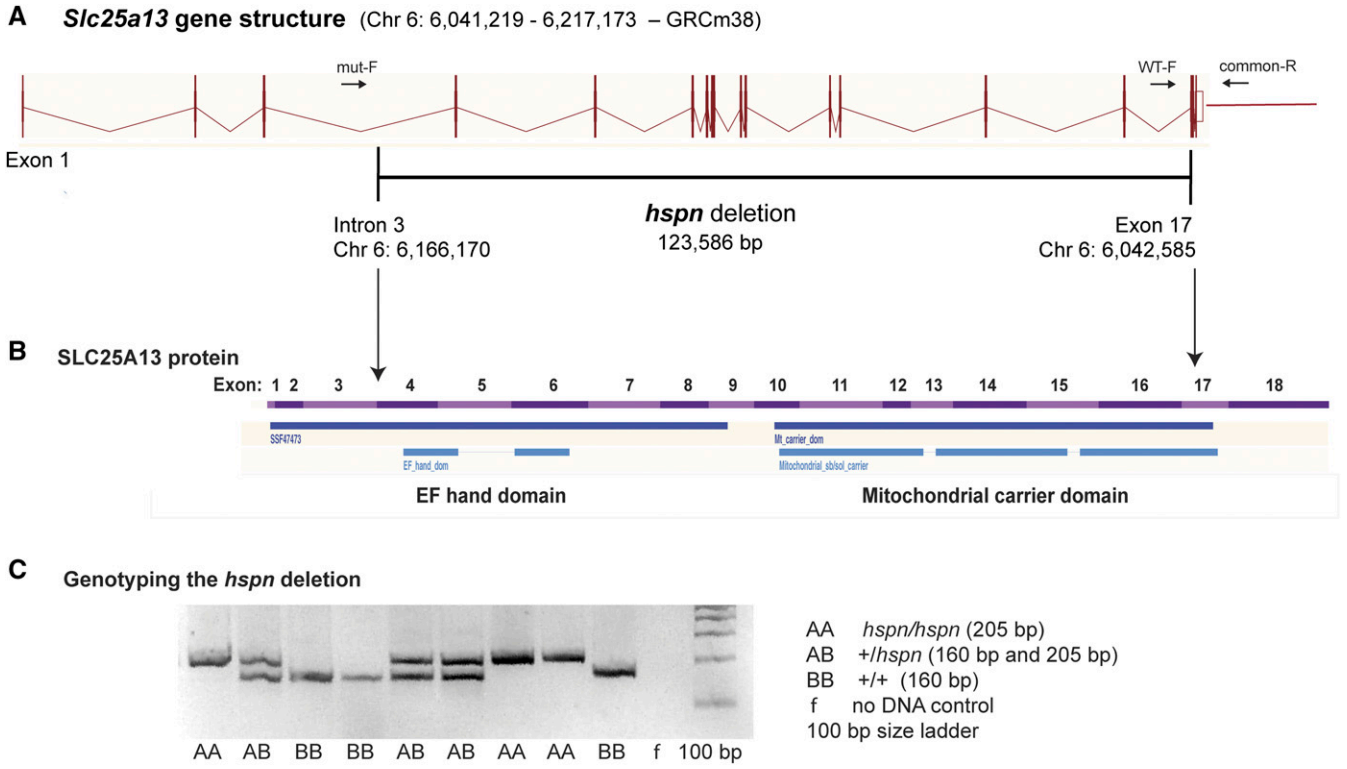

Figure 2 Molecular characterization of the *Slc25a13*^{hspn} mutation. (A) Diagramatic representation of the exon–intron genomic structure of *Slc25a13*. The position of the 123,586-bp *hspn* deletion, extending from intron 3 to exon 17, is shown as a horizontal black line. Positions of PCR primers (mut-F, WT-F, and common-R) used to genotype mice for presence or absence of the *hspn* deletion are shown as ↔. The wild-type allele is amplified with the WT-F forward primer and the common-R reverse primer, and the *hspn* deletion allele is amplified with mut-F and common-R primers. (B) Structural diagram of the SLC25A13 protein. Regions of the protein encoded by the 18 exons of the *Slc25a13* gene are shown as alternating pink and purple bands. Most of the protein is deleted by the *hspn* mutation (indicated by the area between the ↓'s), including both the EF-hand and mitochondrial domains. The structural diagrams for the *Slc25a13* gene and SLC25A13 protein were derived from the Ensembl genome browser. (C) Results from the three-primer PCR assay for the presence or absence of the *hspn* deletion using the mut-F, WT-F, and common-R primers shown in (A). The PCR product size for the *Slc25a13* allele with the *hspn* deletion is 205 bp, and the PCR product size for the wild-type (+) allele is 160 bp; both product sizes are detected in *+/hspn* heterozygotes.

and breakpoints in SHFM1 patients have been associated with isolated SHFM, SHFM with hearing loss, and SHFM with hearing loss and craniofacial abnormalities (Rasmussen *et al.* 2016). Three phenotypic subregions of the SHFM1 locus were identified by the correspondence of these different phenotypes with the sites and extents of the chromosomal aberrations, some of which are shown in Figure 3C. The *Slc25a13*^{hspn} deletion on mouse Chr 6 overlaps with part of the SHFM with hearing loss subregion of the SHFM1 locus (Figure 3D). The different SHFM1 phenotypes resulting from the chromosomal abnormalities are thought to be the result of disruptions of different *cis*-acting elements that regulate tissue-specific expression of *DLX5* and, to a lesser extent, *DLX6*.

Reduced Dlx5 expression in otocysts of Slc25a13$^{hspn/hspn}$ *embryos*

The inner ear phenotype of *Slc25a13*$^{hspn/hspn}$ mice (Figure 1) is very similar to that reported for *Dlx5* knockout mice (Acampora *et al.* 1999; Depew *et al.* 1999; Merlo *et al.* 2002b), which show loss or underdevelopment of semicircular canals and other dorsal inner ear structures. *Dlx6* is less important than *Dlx5* for otic development; inner ears of *Dlx6* knockout mice are like those of wild-type mice, with normal dorsally derived vestibular structures (Jeong *et al.* 2008). To test the hypothesis that regulatory elements located within the *Slc25a13*^{hspn} deletion regulate otic expression of *Dlx5*, we examined *Dlx5* expression in *Slc25a13*$^{hspn/hspn}$ embryos and controls by RNA *in situ* hybridization (Figure 4). *Dlx5* was strongly expressed in the branchial arches and the otic vesicle of wild-type embryos at E9.5 ($N = 5$) and E10.5 ($N = 2$). *Slc25a13*$^{hspn/hspn}$ embryos at E9.5 ($N = 10$) and E10.5 ($N = 4$) also showed strong expression of *Dlx5* in the branchial arches, however, expression in the otic vesicle was much reduced or absent. This expression pattern confirms that the *Slc25a13*^{hspn} deletion has an otic-specific negative effect on *Dlx5* expression, which likely accounts for the similar inner ear phenotypes of *Dlx5*$^{-/-}$ and *Slc25a13*$^{hspn/hspn}$ mutant mice.

Partial lethality of Slc25a13$^{hspn/hspn}$ *mutants and Dlx5*$^{+/-}$ *Slc25a13*$^{hspn/+}$ *transheterozygotes*

Dlx5$^{-/-}$ mice exhibit perinatal lethality. To estimate lethality of *Slc25a13*$^{hspn/hspn}$ homozygotes, we analyzed breeding records for the B6.SJL(c)-*Slc25a13*^{hspn}/Kjn mouse colony. *Slc25a13*$^{+/hspn}$ × *Slc25a13*$^{hspn/hspn}$ (Table 1A) and

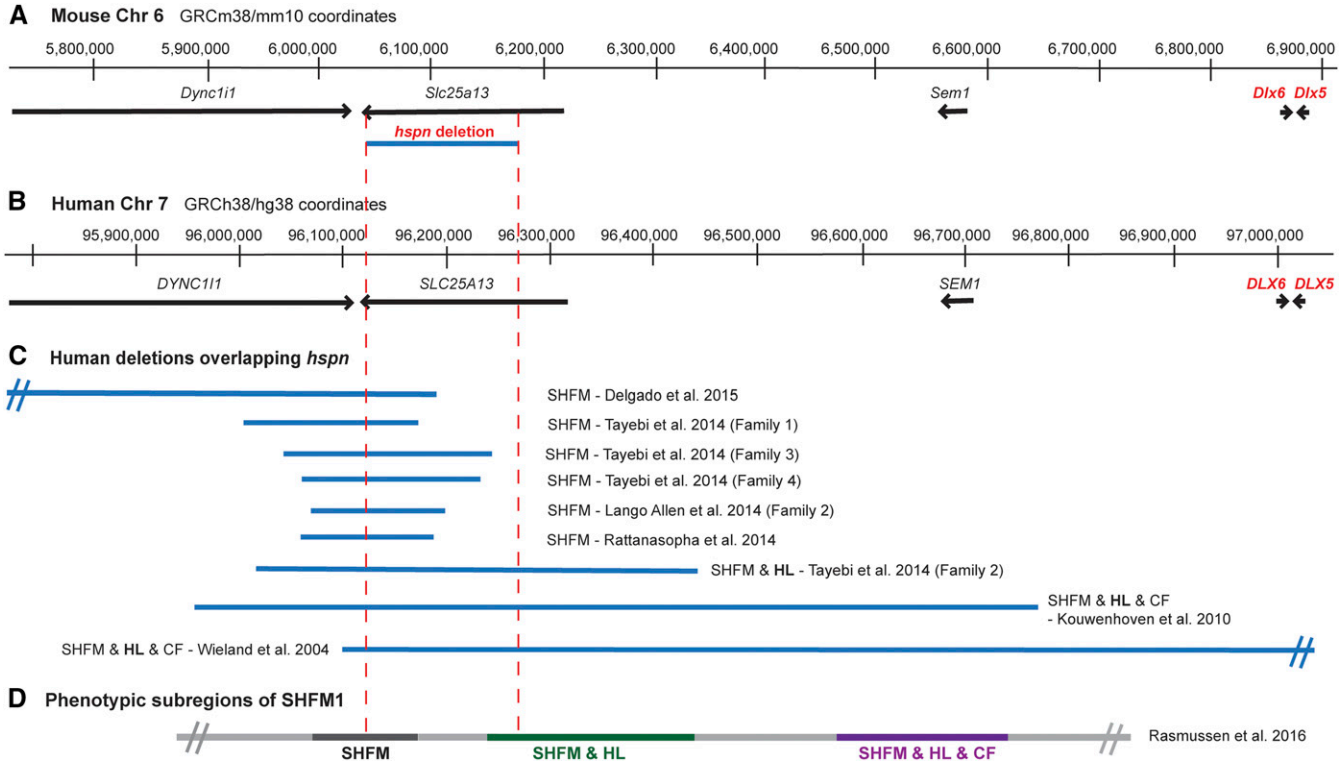

Figure 3 Chr 6 map position of the mouse *Slc25a13*^{hspn} deletion relative to *Dlx5/6* and the corresponding SHFM1 region of human chromosome 7. (A) The region of mouse Chr 6 that corresponds to the human chromosome 7q21.3 region of SHFM1. Positions of the *Dync1i1*, *Slc25a13*, *Shfm1*, *Dlx6*, and *Dlx5* genes are shown as horizontal black lines with arrowheads indicating the direction of transcription. The position of the *Slc25a13*^{hspn} intragenic deletion is shown as a horizontal blue line. (B) The corresponding SHFM1 locus of human chromosome 7. Positions of the *DYNCLI1*, *SLC25A13*, *SEM1*, *DLX6*, and *DLX5* genes are shown as horizontal black lines with arrowheads indicating the direction of transcription. (C) Deletions in SHFM1 patients that overlap with the position of the mouse *Slc25a13*^{hspn} deletion (demarcated by the area between the vertical red dotted lines). The SHFM1 deletions (Wieland *et al.* 2004; Kouwenhoven *et al.* 2010; Lango Allen *et al.* 2014; Rattanasopha *et al.* 2014; Tayebi *et al.* 2014; Delgado and Velinov 2015) were associated with isolated SHFM, SHFM with hearing loss (SHFM & HL), or SHFM with hearing loss and craniofacial abnormalities (SHFM1 & HL & CF). The diverse SHFM1 phenotypes are thought to be the result of disrupted long-range enhancer effects on *DLX5/DLX6* expression. (D) The three phenotypic subregions of the SHFM1 locus inferred from their correlations with chromosomal deletions and inversion break points (Rasmussen *et al.* 2016). The *Slc25a13*^{hspn} deletion overlaps with part of the SHFM & HL subregion.

Slc25a13$^{+/hspn}$ × *Slc25a13*$^{+/hspn}$ (Table 1B) matings both produced lower-than-expected numbers of *Slc25a13*$^{hspn/hspn}$ progeny, with weaning age (3–4 weeks) survival estimates of 28–38% for females and 51–55% for males (Table 1, A and B). For the combined progeny of both matings, the difference in the number of surviving female (57) and male (88) *Slc25a13*$^{hspn/hspn}$ mice was statistically significant (Chi square 6.63, 1 d.f.; $P = 0.01$).

To further test the hypothesis that *cis*-acting regulatory elements deleted by the *hspn* mutation of *Slc25a13* reduce *Dlx5* expression and decrease embryonic viability, we examined phenotypes of mice that were transheterozygous for *Slc25a13*^{hspn} and *Dlx5*$^{-}$ alleles. The B6(Cg)-*Dlx5*$^{tm1(cre/ERT2)Zjh}$/J strain (stock #29895; JAX) was used as our source for the *Dlx5* knockout allele. Progeny were examined from matings of heterozygous *Dlx5*$^{+/-}$ (*Slc25a13*$^{+/+}$) mice with homozygous *Slc25a13*$^{hspn/hspn}$ (*Dlx5*$^{+/+}$) mutant mice (Table 1C). As expected, all 59 progeny produced from these matings were *Slc25a13*$^{+/hspn}$; however, most (54) progeny at weaning age were *Dlx5*$^{+/+}$ rather than *Dlx5*$^{+/-}$, indicating a high rate of lethality for mice that had inherited the *Dlx5*$^{-}$ allele in *trans* configuration with the *Slc25a13*^{hspn} mutation. Only 5 of the 59 progeny produced from this cross were *Dlx5*$^{+/-}$ *Slc25a13*$^{+/hspn}$ transheterozygotes, for an estimated viability at weaning age of only 9% (Table 1C). Although lethality was higher in the transheterozygotes (81%) than in *Slc25a13*$^{hspn/hspn}$ mice (45–72%), it was less severe than that exhibited by *Dlx5*$^{-/-}$ mice, which all die shortly after birth (Acampora *et al.* 1999; Depew *et al.* 1999). *Dlx5*$^{+/-}$ heterozygotes (Table 1D) and *Dlx5*$^{+/-}$ *Slc25a13*$^{+/-}$ transheterozygotes (Table 1E) showed no evidence of lethality at weaning age, demonstrating that it is noncomplementation of the *Slc25a13*^{hspn} and *Dlx5*$^{-}$ mutant alleles that is responsible for *Dlx5*$^{+/-}$ *Slc25a13*$^{+/hspn}$ lethality. These results verify the *cis*-acting nature of the regulatory elements deleted by the *Slc25a13*^{hspn} mutation.

Inner ear phenotype of Dlx5$^{+/-}$ *Slc25a13*$^{+/hspn}$ *transheterozygotes*

Only 5 out of a total of 59 progeny produced from *Dlx5*$^{+/-}$ × *Slc25a13*$^{hspn/hspn}$ matings were *Dlx5*$^{+/-}$ *Slc25a13*$^{+/hspn}$ transheterozygotes (Table 1C), and these were the only ones that exhibited a pronounced circling and head-bobbing

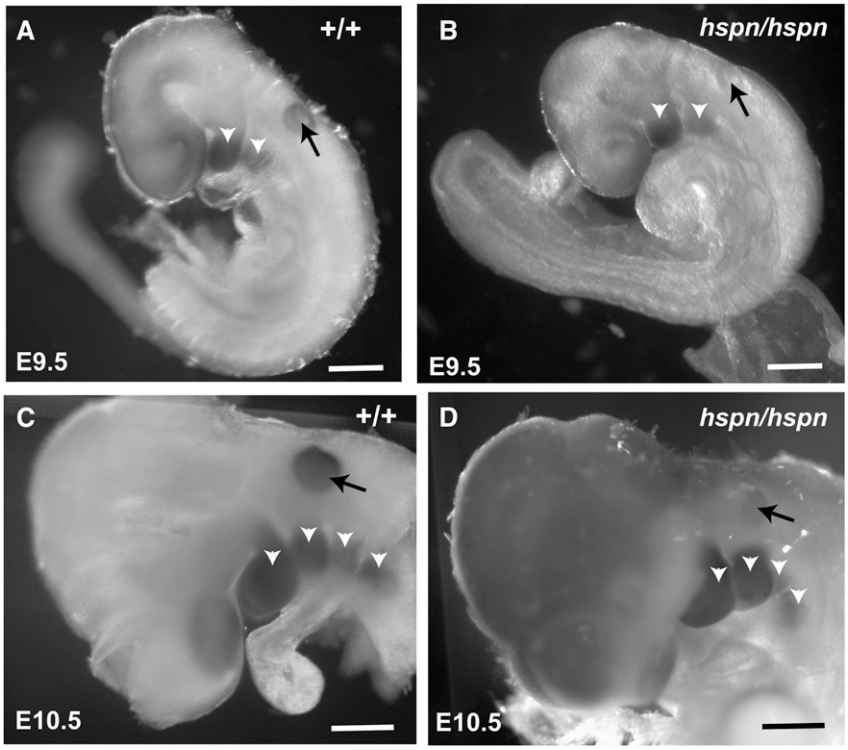

Figure 4 Decreased *Dlx5* expression in the otic vesicle of *Slc25a13*$^{hspn/hspn}$ embryos. Whole mounts of embryos were hybridized with a *Dlx5* antisense RNA probe. Wild-type *Slc25a13* (+/+) embryos at E9.5 (A) and E10.5 (C) showed expression of *Dlx5* in the branchial arches (open arrowheads) and in the otic vesicle (solid arrows). Although *Slc25a13*$^{hspn/hspn}$ (*hspn/hspn*) mutant embryos (B and D) showed strong *Dlx5* expression in the branchial arches, expression appeared absent in the otic vesicle at E9.5 (B) and severely reduced in the otic vesicle at E10.5 (D). Bars, 500 μm.

phenotype indicating inner ear dysfunction. We tested these five mice at 5–10 weeks of age for ABR thresholds and examined the morphology of their inner ears. All of the transheterozygotes were deaf with no detectable ABR even at the maximum 100-dB SPL test stimulus (Figure 5A). Their inner ears were grossly malformed with undeveloped dorsal structures and enlarged cochlear ducts (Figure 5B), a phenotype similar to that of adult *Slc25a13*$^{hsp/hspn}$ mice (Figure 1B). In contrast, all 20 *Dlx5*$^{+/-}$ *Slc25a13*$^{+/-}$ transheterozygotes produced from *Dlx5*$^{+/-}$ × *Slc25a13*$^{-/-}$ matings had normal ABR thresholds at 5–8 weeks of age.

Survival and inner ear morphology was also examined in E15.5 embryos from a timed mating of *Dlx5*$^{+/-}$ and *Slc25a13*$^{hspn/hspn}$ mice. Of 13 embryos produced from two litters, 7 were genotyped as *Dlx5*$^{+/+}$ *Slc25a13*$^{+/hspn}$ and 6 as *Dlx5*$^{+/-}$ *Slc25a13*$^{+/hspn}$; demonstrating normal survival at this age. Paintfills of four inner ears from two E15.5 *Dlx5*$^{+/+}$ *Slc25a13*$^{+/hspn}$ controls showed normal morphology (Figure 5C), whereas four inner ears from two littermate *Dlx5*$^{+/-}$ *Slc25a13*$^{+/hspn}$ transheterozygotes lacked dorsal structures and had malformed and thickened cochlear ducts (Figure 5, D and E), similar to the inner ears of *Slc25a13*$^{hsp/hspn}$ (Figure 1A) and *Dlx5*$^{-/-}$ (Depew *et al.* 1999; Merlo *et al.* 2002b) embryos. Paintfill analysis revealed some variability in the inner ear phenotype of the E15.5 *Dlx5*$^{+/-}$ *Slc25a13*$^{+/hspn}$ transheterozygotes, with inner ears from one of the two embryos examined showing development of the endolymphatic sac and duct (Figure 5E). We conclude that the inner ear malformations of *Dlx5*$^{+/-}$ *Slc25a13*$^{+/hspn}$ transheterozygotes are caused by a severe reduction in *Dlx5* expression during otic development, which results from a loss of *cis*-regulatory *Dlx5* enhancer elements on one chromosome (the *Slc25a13*^{hspn} deletion) combined with a loss of a functional *Dlx5* allele on the other chromosome (the *Dlx5*$^{-}$ knockout mutation).

In vivo deletion analysis of putative Dlx5 enhancer elements

We deleted two subregions of the *hspn* deletion that contain putative enhancer elements and tested the *in vivo* effects of these subdeletions on inner ear function. We used CRISPR/Cas9-mediated genome editing in C57BL/6J zygotes to produce separate deletions corresponding to two putative *Dlx5* enhancer elements (hs1642 and hs2313) located within the genomic region deleted by the *Slc25a13*^{hspn} mutation (Figure 6). The hs1642 and hs2313 elements are included in the VISTA Enhancer Browser (Visel *et al.* 2007), a resource for experimentally validated human and mouse noncoding fragments with gene enhancer activity assessed by reporter gene expression in transgenic mice. In assays of E11.5 mouse embryos, the hs1642 element showed enhancer activity in forebrain, hindbrain, and neural tube; and the hs2313 element, equivalent to the eDlx#23 enhancer (Birnbaum *et al.* 2012), showed enhancer activity in the otic vesicle, forebrain, branchial arch, and limb bud. Deletions of hs1642 (Δhs1642) and hs2313 (Δhs2313) were verified by DNA sequence analysis, and separate homozygous mouse strains were developed for each deletion. Details of the deletions and mouse strains are given in Table S1. All mice examined from the hs1642 and hs2313 deletion strains showed normal morphology and behavior, with no indications of vestibular dysfunction. Three

Table 1 Viability estimates for *Slc25a13*$^{hspn/hspn}$ and *Dlx5*$^{+/-}$ *Slc25a13*$^{+/hspn}$ mice at weaning age

Observed number of progeny for each genotype		Expected genotype ratio	Chi square (probability)	Semilethal genotype: Expected number[a]	Semilethal genotype: Estimated viability[b] (%)
A. Mating: *Slc25a13*$^{+/hspn}$ × *Slc25a13*$^{hspn/hspn}$					
Slc25a13$^{hspn/hspn}$	*Slc25a13*$^{+/hspn}$	1:1		*Slc25a13*$^{hspn/hspn}$	
Female 36	128		51.6 ($P < 0.0001$)	128	28
Male 57	103		13.2 ($P < 0.005$)	103	55
B. Mating: *Slc25a13*$^{+/hspn}$ × *Slc25a13*$^{+/hspn}$					
Slc25a13$^{hspn/hspn}$	*Slc25a13*$^{+/+}$ or $^{+/hspn}$	1:3		*Slc25a13*$^{hspn/hspn}$	
Female 21	168		19.4 ($P < 0.0001$)	56	38
Male 31	182		12.4 ($P < 0.005$)	60.7	51
C. Mating: *Dlx5*$^{+/-}$ × *Slc25a13*$^{hspn/hspn}$					
Dlx5$^{+/-}$ *Slc25a13*$^{+/hspn}$	*Dlx5*$^{+/+}$ *Slc25a13*$^{+/hspn}$	1:1		*Dlx5*$^{+/KO}$ *Slc25a13*$^{+/hspn}$	
5 (3 females, 2 males)	54 (24 females, 30 males)		40.7 ($P < 0.0001$)	54	9
D. Mating: *Dlx5*$^{+/-}$ × *Dlx5*$^{+/+}$					
Dlx5$^{+/-}$	*Dlx5*$^{+/+}$	1:1		No significant difference	
76	69		0.34 ($P > 0.5$)		
E. Mating: *Dlx5*$^{+/-}$ × *Slc25a13*$^{-/-}$					
Dlx5$^{+/-}$ *Slc25a13*$^{+/-}$	*Dlx5*$^{+/+}$ *Slc25a13*$^{+/-}$	1:1		No significant difference	
6	6		0 ($P > 0.9$)		

[a] Expected number of progeny if no lethality.
[b] Observed/expected number × 100.

mice from the hs1642 deletion strain and four from the hs2313 deletion strain were tested for ABR thresholds at 2–3 months of age, and all exhibited normal thresholds similar to those of age-matched controls. To test for *cis*-regulatory effects of the putative enhancer deletions, *Slc25a13* $^{\Delta hs1642/\Delta hs1642}$ and *Slc25a13* $^{\Delta hs2313/\Delta hs2313}$ mice were crossed with *Dlx5*$^{+/-}$ mice. All transheterozygous mice produced from these crosses (18 *Slc25a13*$^{+/\Delta hs1642}$ *Dlx5*$^{+/-}$ and 11 *Slc25a13*$^{+/\Delta hs3213}$ *Dlx5*$^{+/-}$) showed normal behavior and normal ABR thresholds when tested at 4–13 weeks of age.

Because homozygous deletions of the hs1642 and hs2313 elements had no detectable negative phenotypic effects, we used CRISPR/Cas9 genome editing to produce larger (25 kb) deletions within the *hspn*-deleted region of *Slc25a13*. The deletions targeted the 6,142,000- 6,166,000-bp segment of mouse Chr 6 (GRCm38), chosen because it contains a phylogenetically conserved region in intron 4 of the *Slc25a13* gene as well as the putative hs1642 enhancer element (Figure 6), and because the deletion covers the only region of the *hspn* deletion that overlaps with the corresponding region of the human SHFM1 locus predicted to associate with hearing loss (Figure 3). Three independent inbred strains of mice (line 6, line 12, and line 54) were produced that span the 25-kb targeted region of mouse Chr 6, and details of these strains and their deletions are given in Table S1. None of the mice from these homozygous deletion strains exhibited behaviors suggestive of vestibular dysfunction. A total of 10 mice from line 6, 3 from line 12, and 6 from line 54 were evaluated for hearing at 1–4 months of age, and all exhibited normal ABR thresholds.

The lack of any discernable vestibular or auditory dysfunction in mice from the strains listed in Table S1 indicates that the individual deletions of the putative enhancer regions are not by themselves responsible for the inner ear dysfunction of *Slc25a13*$^{hspn/hspn}$ mice.

Discussion

We present several lines of evidence demonstrating that the mutation underlying the congenital hearing loss, vestibular dysfunction, and dysmorphic inner ears of *hspn* mutant mice is a large intragenic deletion extending from within intron 3–4 to exon 17 of *Slc25a13*. First, the *hspn* mutation was mapped to a genomic interval that contains the *Slc25a13* gene, and upon DNA sequencing of all exons in the genetically determined candidate region, only the *Slc25a13* gene was mutated. Second, the chromosomal deletion identified in *hspn* genomic DNA is confined to a region within the *Slc25a13* gene. Third, there is complete concordance between the mutant mouse phenotype and homozygosity for the *Slc25a13* intragenic deletion in all mice examined. Nonetheless, there is a possibility that extraexonic sequence alterations outside of the *Slc25a13* deletion, but still within the genetically defined critical region of the *hspn* mutation, may actually be responsible for the dysregulation of the downstream *Dlx5* gene. However, because the spontaneous *hspn* mutation occurred recently in an inbred strain, only a single DNA sequence difference is expected between the coisogenic mutant strain and the control strain.

The inner ear abnormalities of *Slc25a13*$^{hspn/hspn}$ mutant mice (Figure 1) are similar to those reported for SHFM1 patients with hearing loss (Haberlandt *et al.* 2001; Wieland *et al.* 2004), with variable loss of vestibular structures and a thick, but shortened, cochlear duct. They are likewise similar to the inner ear defects of *Dlx5* knockout mice (Acampora *et al.* 1999; Depew *et al.* 1999; Merlo *et al.* 2002b). Although

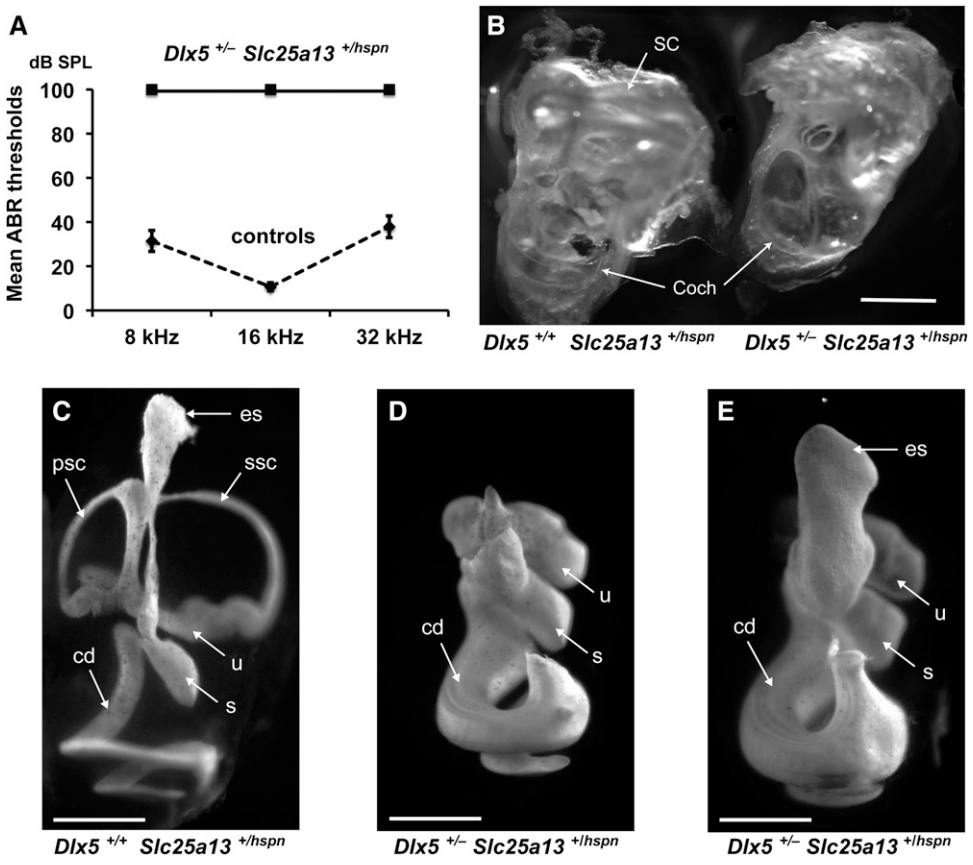

Figure 5 The phenotype of *Dlx5*$^{+/-}$ *Slc25a13*$^{+/hspn}$ transheterozygotes is similar to that of *Dlx5*$^{-/-}$ knockout mice. (A) Mice between 5 and 10 weeks of age were tested for ABR thresholds at 8-, 16-, and 32-kHz frequencies. All three *Dlx5*$^{+/-}$ *Slc25a13*$^{+/hspn}$ transheterozygotes lacked ABRs even at the highest test stimulus (100-dB SPL), whereas all eight control mice (three *Dlx5*$^{+/+}$ *Slc25a13*$^{+/+}$, two *Dlx5*$^{+/+}$ *Slc25a13*$^{+/hspn}$, and three *Dlx5*$^{+/-}$ *Slc25a13*$^{+/+}$) exhibited normal thresholds. Error bars represent SD. (B) Cleared inner ears from an adult (10 weeks old) *Dlx5*$^{+/+}$ *Slc25a13*$^{+/hspn}$ control and a *Dlx5*$^{+/-}$ *Slc25a13*$^{+/hspn}$ transheterozygous littermate. Inner ears of *Dlx5*$^{+/-}$ *Slc25a13*$^{+/hspn}$ transheterozygotes lack fully developed semicircular canals (SC) and have a malformed cochlea (Coch) with enlarged duct. Bar, 1 mm. (C–E) Paintfills of the membranous labyrinths of inner ears from E15.5 embryos. Inner ears of *Dlx5*$^{+/+}$ *Slc25a13*$^{+/hspn}$ controls (C) have normal morphology, whereas inner ears of *Dlx5*$^{+/-}$ *Slc25a13*$^{+/hspn}$ transheterozygotes (D and E) lack dorsal structures and have malformed and thickened cochlear ducts. An enlarged endolymphatic sac was seen in one (E) but not all (D) inner ears of transheterozygotes. cd, cochlear duct; es, endolymphatic sac; psc, posterior semicircular canal; s, saccule; ssc, superior semicircular canal; u, utricle. Bars, 0.5 mm.

Dlx5 and *Dlx6* appear to be functionally redundant for jaw development, *Dlx6* is less important than *Dlx5* for otic development, and inner ears of *Dlx6* knockout mice appear similar to those of wild-type mice, with normal vestibular structures (Jeong *et al.* 2008). The dorsal otocyst, where *Dlx5* is expressed, gives rise to the anterior and posterior semicircular canals and the endolymphatic duct. Consistent with this developmental pattern, the saccule and cochlea of *Dlx5* knockout and *Slc25a13*$^{hspn/hspn}$ mice appear less affected than the vestibular apparatus, which is very reduced in size with loss of or incorrectly formed semicircular canals and endolymphatic duct. In *Dlx5* knockout mice (Acampora *et al.* 1999; Depew *et al.* 1999; Merlo *et al.* 2002b), as in *Slc25a13*$^{hspn/hspn}$ mutant mice (Figure 1), the severity of dysmorphology of the inner ears varies among individual mutants, even on inbred strain backgrounds.

Here we show by RNA *in situ* hybridization analysis that *Dlx5* expression is greatly reduced or absent in the otic vesicle of *Slc25a13*$^{hspn/hspn}$ embryos (Figure 4), and that *Dlx5*$^{+/-}$ *Slc2a13*$^{+/hspn}$ transheterozygotes are deaf with malformed inner ears (Figure 5). Together, these results provide strong evidence that the loss of *cis*-acting regulatory elements located in the *Slc25a13*^{hspn} gene reduce *Dlx5* expression and are responsible for the dysmorphic inner ears and deafness of *Slc25a13*$^{hspn/hspn}$ mutant mice. Non-otic abnormalities that are commonly observed in mice homozygous for targeted *Dlx5* knockout mutations, such as multiple defects of craniofacial structures (Acampora *et al.* 1999; Depew *et al.* 1999; Merlo *et al.* 2002b), are not observed in *Slc25a13*$^{hspn/hspn}$ mice. This is likely due to the fact that the regulatory elements deleted by the *hspn* mutation are specific to *Dlx5* expression in the developing inner ear, as evidenced by loss of *Dlx5* expression in the otocyst but not the branchial arches of *Slc25a13*$^{hspn/hspn}$ embryos (Figure 4). Although the *Slc25a13*^{hspn} deletion is located ~700 kb away from *Dlx5*, there is precedence for such long-range noncoding elements having regulatory effects on gene expression (Kleinjan and van Heyningen 2005; Noonan and McCallion 2010). For example, another developmentally important gene, *Shh*, has a long-range enhancer located 1 Mb away—in the intron of another gene—that regulates expression in the developing limb (Lettice *et al.* 2003).

Only ~30% of female and 50% of male *Slc25a13*$^{hspn/hspn}$ mice survive to weaning age (Table 1). To account for this 50–70% lethality, *Dlx5* expression in *Slc25a13*$^{hspn/hspn}$ mice must be detrimentally reduced in another organ during development that is more critical for viability than the inner ear. *Dlx5* is expressed in many organ systems at various stages of embryonic development, but a definitive cause for neonatal death in *Dlx5* knockout mice has not been determined (Depew *et al.* 1999). The *Dlx5* expression levels related to

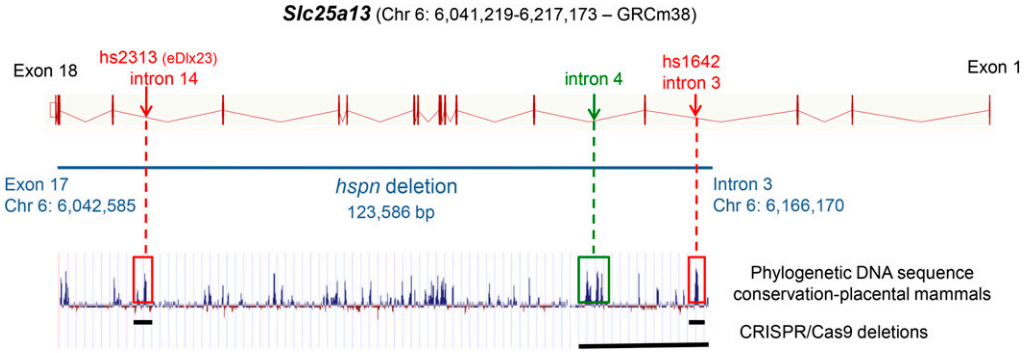

Figure 6 Putative enhancer elements within the *Slc25a13*^{hspn} deletion. Locations of two putative enhancer elements, hs2313 (Chr6: 6,058,554–6,059,028; GRCm38) and hs1642 (Chr 6: 6,163,229–6,163,674), that lie within the *hspn*-deleted region (shown as horizontal blue line) of *Slc25a13* were obtained from the VISTA Enhancer Browser (http://enhancer-test.lbl.gov/frnt_page.shtml). The hs2313 element is equivalent to the eDlx#23 enhancer (Birnbaum *et al.* 2012). DNA sequences of both elements show a high degree of phylogenic conservation for noncoding DNA (peaks enclosed by red boxes). An additional noncoding region of high sequence conservation occurs in intron 4 (peak enclosed by green box). Specific deletions corresponding to these conserved regions were created using CRISPR/Cas9 genome editing, and the extent of these deletions are shown by horizontal black lines at the bottom of the figure. The gene structure diagram for *Slc25a13* is derived from the Ensembl genome browser, and the phylogenetic conservation diagram is from the University of California, Santa Cruz Genome Browser comparative genomics track.

lethality appear to be dosage sensitive because lethality at weaning age is 50–70% in *Slc25a13*$^{hspn/hspn}$ mice, 90% in *Dlx5*$^{+/-}$ *Slc2a13*$^{+/hspn}$ transheterozygotes (Table 1), and 100% in *Dlx5*$^{-/-}$ knockout mice shortly after birth (Acampora *et al.* 1999; Depew *et al.* 1999; Merlo *et al.* 2002b).

Slc25a13 (Sinasac *et al.* 1999; del Arco *et al.* 2002; Birnbaum *et al.* 2012), *Sem1* (Birnbaum *et al.* 2012), and *Dlx5* (Acampora *et al.* 1999; Depew *et al.* 1999) are similarly expressed in branchial arches, limb bud, and otic vesicle of mouse embryos, yet expression in these tissues appears functionally important only for *Dlx5*. Expression of *Slc25a13* in these tissues seems to be dispensable and may be an inadvertent consequence of its genomic location. The similar expression patterns of *Slc25a13* and *Dlx5*, which have nothing in common except for their genomic location, suggests that they may be located in a regulatory landscape wherein tissue-specific coexpression of genes (which may or may not be functionally related) is regulated by a common control region or group of long-range enhancers, as has been described for the chromosomal regions around the mouse *HoxD* gene cluster (Spitz *et al.* 2003) and the *Grem1* gene (Zuniga *et al.* 2004). Genomic clustering of coexpressed genes may be widespread in genomes, particularly in regions around developmental control genes (Spitz and Duboule 2008), and may correspond with topologically associating domains (Dekker and Heard 2015).

The *SLC25A13* region homologous to the *Slc25a13*^{hspn} deletion is included in the SHFM1 minimal region and overlaps with the subregion that is associated with hearing loss (Figure 3). Multiple long-range, tissue-specific enhancer elements that presumably regulate *DLX5/6* expression have been identified at various sites in the SHFM1 locus that correspond with the limb, inner ear, and craniofacial abnormalities associated with this syndrome (Birnbaum *et al.* 2012). These putative enhancer elements were identified by their high degree of DNA sequence conservation across species (at least 77% identity for ≥100 bp between human and frog) followed by transgenic expression assays in zebrafish and mouse. The *Slc25a13*^{hspn} deletion contains two of these putative enhancer elements, eDlx#23 (hs2313) and hs1642 (Figure 6). eDlx#23 enhanced reporter gene activity in the otic vesicle, forebrain, branchial arch, and limb bud, and was suggested to regulate *DLX5* expression and underlie the hearing loss associated with some SHFM1 families (Birnbaum *et al.* 2012). Later studies, however, have described multiple SHFM1 families with deletions that include the eDlx#23 enhancer element but that do not exhibit hearing loss, indicating that deletion of eDlx#23 is not by itself responsible for SHFM1-associated hearing loss (Lango Allen *et al.* 2014; Rattanasopha *et al.* 2014; Tayebi *et al.* 2014; Delgado and Velinov 2015). Although the hs1642 enhancer element is present in all SHFM1 deletions associated with hearing loss, it does not show enhanced reporter gene activity in the otic vesicle of mouse embryos.

To directly test the functional importance of specific candidate enhancers *in vivo*, we used CRISPR/Cas9 genome editing to make deletions of the phylogenetically conserved eDlx#23 and hs1642 elements and also a deletion of a larger 25-kb DNA region containing additional conserved sequences (Figure 6 and Table S1). Mice homozygous for each of the putative enhancer deletions had no obvious phenotypic abnormalities and exhibited normal hearing. Deletions of other highly conserved elements, which also show *in vivo* enhancer activity in mouse transgenic assays, have likewise yielded mice without any noticeable abnormalities (Ahituv *et al.* 2007). The negative results from these studies demonstrate that transgenic enhancer assays do not reliably predict phenotypic relevance and may indicate that the conserved elements have a redundant regulatory function. Multiple and possibly redundant *cis*-enhancer elements appear to be pervasive in regulating developmental pathways (Cannavo *et al.* 2016). For example, multiple *cis*-regulatory elements, some of them partially redundant, have been located in a 1-Mb region upstream of *POU3F4* and promote its expression during inner ear development (Naranjo *et al.* 2010). Additional CRISPR/Cas9-mediated subdeletions of

the *Slc25a13*^{hspn} deletion or multiple combinations of subdeletions may be needed to reduce *Dlx5* expression enough to affect inner ear development. Across-species sequence conservation is not always a consistent feature of enhancers (Noonan and McCallion 2010), and less conserved sequences within the *Slc25a13*^{hspn} deletion may also contribute to enhancer function. In addition to DNA sequence conservation, there are other means that could be employed to identify potential enhancer elements, including transcription factor binding sites, DNase hypersensitive sites, and chromatin immunoprecipitation sequencing for histone modifications and p300-bound regions (Shlyueva *et al.* 2014). The deletion strains listed in Table S1 provide valuable starting materials for future attempts to identify such enhancer elements.

In summary, we show here that loss of *cis*-regulatory elements within the *Slc25a13*^{hspn} deletion decreases *Dlx5* expression in the otic vesicle and is responsible for the inner ear dysmorphology and hearing loss of *Slc25a13*$^{hspn/hspn}$ mutant mice. *Slc25a13*$^{hspn/hspn}$ mice are viable as adults, in contrast to the perinatal lethality of *Dlx5* knockout mice, and therefore can be used to study later-occurring effects of reduced *Dlx5* expression in the inner ear. Our results in mice suggest that long-range *DLX5* enhancer elements located in the human *SLC25A13* gene may underlie the sensorineural hearing loss that is sometimes associated with SHFM1. The lack of limb or craniofacial abnormalities in *Slc25a13*$^{hspn/hspn}$ mice also suggests that disruptions of otic-specific *DLX5* enhancers may underlie some cases of human nonsyndromic hearing impairment. The *Slc25a13*^{hspn} mice provide a new model system for studying distal-acting enhancer elements that regulate *Dlx5* expression during inner ear development.

Acknowledgments

We thank Sandra Gray for general mouse colony management and for the generation of linkage-cross mice and Cindy Avery of the Technology Evaluation and Development group for husbandry assistance with the mouse CRISPR deletion strains. We thank personnel of The Jackson Laboratory's Genetic Engineering Technologies service for generation of the *Slc25a13* knockout mouse and Pete Finger of the Electron Microscopy Service for tissue preparation and processing for scanning electron microscopy. This study was supported by US National Institutes of Health grant R01 DC-004301 (to K.R.J.). The Jackson Laboratory shared services are supported by National Institutes of Health grant P30 CA-034196.

Literature Cited

Acampora, D., G. R. Merlo, L. Paleari, B. Zerega, M. P. Postiglione *et al.*, 1999 Craniofacial, vestibular and bone defects in mice lacking the distal-less-related gene Dlx5. Development 126: 3795–3809.

Ahituv, N., Y. Zhu, A. Visel, A. Holt, V. Afzal *et al.*, 2007 Deletion of ultraconserved elements yields viable mice. PLoS Biol. 5: e234.

Bernardini, L., C. Palka, C. Ceccarini, A. Capalbo, I. Bottillo *et al.*, 2008 Complex rearrangement of chromosomes 7q21.13-q22.1 confirms the ectrodactyly-deafness locus and suggests new candidate genes. Am. J. Med. Genet. A. 146A: 238–244.

Birnbaum, R. Y., D. B. Everman, K. K. Murphy, F. Gurrieri, C. E. Schwartz *et al.*, 2012 Functional characterization of tissue-specific enhancers in the DLX5/6 locus. Hum. Mol. Genet. 21: 4930–4938.

Brown, K. K., J. A. Reiss, K. Crow, H. L. Ferguson, C. Kelly *et al.*, 2010 Deletion of an enhancer near DLX5 and DLX6 in a family with hearing loss, craniofacial defects, and an inv(7)(q21.3q35). Hum. Genet. 127: 19–31.

Bulger, M., and M. Groudine, 2011 Functional and mechanistic diversity of distal transcription enhancers. Cell 144: 327–339.

Cannavo, E., P. Khoueiry, D. A. Garfield, P. Geeleher, T. Zichner *et al.*, 2016 Shadow enhancers are pervasive features of developmental regulatory networks. Curr. Biol. 26: 38–51.

Contreras, L., P. Gomez-Puertas, M. Iijima, K. Kobayashi, T. Saheki *et al.*, 2007 Ca2+ Activation kinetics of the two aspartate-glutamate mitochondrial carriers, aralar and citrin: role in the heart malate-aspartate NADH shuttle. J. Biol. Chem. 282: 7098–7106.

Coppola, C. J., R. C. Ramaker, and E. M. Mendenhall, 2016 Identification and function of enhancers in the human genome. Hum. Mol. Genet. 25: R190–R197.

Daniel, B., G. Nagy, and L. Nagy, 2014 The intriguing complexities of mammalian gene regulation: how to link enhancers to regulated genes. Are we there yet? FEBS Lett. 588: 2379–2391.

Dekker, J., and E. Heard, 2015 Structural and functional diversity of topologically associating domains. FEBS Lett. 589: 2877–2884.

del Arco, A., J. Morcillo, J. R. Martinez-Morales, C. Galian, V. Martos *et al.*, 2002 Expression of the aspartate/glutamate mitochondrial carriers aralar1 and citrin during development and in adult rat tissues. Eur. J. Biochem. 269: 3313–3320.

Delgado, S., and M. Velinov, 2015 7q21.3 Deletion involving enhancer sequences within the gene DYNC1I1 presents with intellectual disability and split hand-split foot malformation with decreased penetrance. Mol. Cytogenet. 8: 37.

Depew, M. J., J. K. Liu, J. E. Long, R. Presley, J. J. Meneses *et al.*, 1999 Dlx5 regulates regional development of the branchial arches and sensory capsules. Development 126: 3831–3846.

Fu, Y., J. D. Sander, D. Reyon, V. M. Cascio, and J. K. Joung, 2014 Improving CRISPR-Cas nuclease specificity using truncated guide RNAs. Nat. Biotechnol. 32: 279–284.

Haberlandt, E., J. Loffler, A. Hirst-Stadlmann, B. Stockl, W. Judmaier *et al.*, 2001 Split hand/split foot malformation associated with sensorineural deafness, inner and middle ear malformation, hypodontia, congenital vertical talus, and deletion of eight microsatellite markers in 7q21.1-q21.3. J. Med. Genet. 38: 405–409.

Hulander, M., A. E. Kiernan, S. R. Blomqvist, P. Carlsson, E. J. Samuelsson *et al.*, 2003 Lack of pendrin expression leads to deafness and expansion of the endolymphatic compartment in inner ears of Foxi1 null mutant mice. Development 130: 2013–2025.

Ignatius, J., S. Knuutila, S. W. Scherer, B. Trask, and J. Kere, 1996 Split hand/split foot malformation, deafness, and mental retardation with a complex cytogenetic rearrangement involving 7q21.3. J. Med. Genet. 33: 507–510.

Jeong, J., X. Li, R. J. McEvilly, M. G. Rosenfeld, T. Lufkin *et al.*, 2008 Dlx genes pattern mammalian jaw primordium by regulating both lower jaw-specific and upper jaw-specific genetic programs. Development 135: 2905–2916.

Kiernan, A. E., 2006 The paintfill method as a tool for analyzing the three-dimensional structure of the inner ear. Brain Res. 1091: 270–276.

Kim, H. M., and P. Wangemann, 2010 Failure of fluid absorption in the endolymphatic sac initiates cochlear enlargement that

leads to deafness in mice lacking pendrin expression. PLoS One 5: e14041.
Kleinjan, D. A., and V. van Heyningen, 2005 Long-range control of gene expression: emerging mechanisms and disruption in disease. Am. J. Hum. Genet. 76: 8–32.
Kopecky, B., P. Santi, S. Johnson, H. Schmitz, and B. Fritzsch, 2011 Conditional deletion of N-Myc disrupts neurosensory and non-sensory development of the ear. Dev. Dyn. 240: 1373–1390.
Kouwenhoven, E. N., S. J. van Heeringen, J. J. Tena, M. Oti, B. E. Dutilh *et al.*, 2010 Genome-wide profiling of p63 DNA-binding sites identifies an element that regulates gene expression during limb development in the 7q21 SHFM1 locus. PLoS Genet. 6: e1001065.
Lango Allen, H., R. Caswell, W. Xie, X. Xu, C. Wragg *et al.*, 2014 Next generation sequencing of chromosomal rearrangements in patients with split-hand/split-foot malformation provides evidence for DYNC1I1 exonic enhancers of DLX5/6 expression in humans. J. Med. Genet. 51: 264–267.
Lettice, L. A., S. J. Heaney, L. A. Purdie, L. Li, P. de Beer *et al.*, 2003 A long-range Shh enhancer regulates expression in the developing limb and fin and is associated with preaxial polydactyly. Hum. Mol. Genet. 12: 1725–1735.
Liu, P., N. A. Jenkins, and N. G. Copeland, 2003 A highly efficient recombineering-based method for generating conditional knockout mutations. Genome Res. 13: 476–484.
Lorente-Canovas, B., N. Ingham, E. E. Norgett, Z. J. Golder, F. E. Karet Frankl *et al.*, 2013 Mice deficient in H+-ATPase a4 subunit have severe hearing impairment associated with enlarged endolymphatic compartments within the inner ear. Dis. Model. Mech. 6: 434–442.
Low, B. E., P. M. Kutny, and M. V. Wiles, 2016 Simple, efficient CRISPR-Cas9-mediated gene editing in mice: strategies and methods. Methods Mol. Biol. 1438: 19–53.
Ma, Q., D. J. Anderson, and B. Fritzsch, 2000 Neurogenin 1 null mutant ears develop fewer, morphologically normal hair cells in smaller sensory epithelia devoid of innervation. J. Assoc. Res. Otolaryngol. 1: 129–143.
Marinoni, J. C., R. E. Stevenson, J. P. Evans, D. Geshuri, M. C. Phelan *et al.*, 1995 Split foot and developmental retardation associated with a deletion of three microsatellite markers in 7q21.2-q22.1. Clin. Genet. 47: 90–95.
Merlo, G. R., L. Paleari, S. Mantero, F. Genova, A. Beverdam *et al.*, 2002a Mouse model of split hand/foot malformation type I. Genesis 33: 97–101.
Merlo, G. R., L. Paleari, S. Mantero, B. Zerega, M. Adamska *et al.*, 2002b The Dlx5 homeobox gene is essential for vestibular morphogenesis in the mouse embryo through a BMP4-mediated pathway. Dev. Biol. 248: 157–169.
Naranjo, S., K. Voesenek, E. de la Calle-Mustienes, A. Robert-Moreno, H. Kokotas *et al.*, 2010 Multiple enhancers located in a 1-Mb region upstream of POU3F4 promote expression during inner ear development and may be required for hearing. Hum. Genet. 128: 411–419.
Noonan, J. P., and A. S. McCallion, 2010 Genomics of long-range regulatory elements. Annu. Rev. Genomics Hum. Genet. 11: 1–23.
Palmieri, L., B. Pardo, F. M. Lasorsa, A. del Arco, K. Kobayashi *et al.*, 2001 Citrin and aralar1 are Ca(2+)-stimulated aspartate/glutamate transporters in mitochondria. EMBO J. 20: 5060–5069.
Pauley, S., E. Lai, and B. Fritzsch, 2006 Foxg1 is required for morphogenesis and histogenesis of the mammalian inner ear. Dev. Dyn. 235: 2470–2482.
Piette, D., M. Hendrickx, E. Willems, C. R. Kemp, and L. Leyns, 2008 An optimized procedure for whole-mount in situ hybridization on mouse embryos and embryoid bodies. Nat. Protoc. 3: 1194–1201.
Rasmussen, M. B., S. Kreiborg, P. Jensen, M. Bak, Y. Mang *et al.*, 2016 Phenotypic subregions within the split-hand/foot malformation 1 locus. Hum. Genet. 135: 345–357.
Rattanasopha, S., S. Tongkobpetch, C. Srichomthong, P. Kitidumrongsook, K. Suphapeetiporn *et al.*, 2014 Absent expression of the osteoblast-specific maternally imprinted genes, DLX5 and DLX6, causes split hand/split foot malformation type I. J. Med. Genet. 51: 817–823.
Robledo, R. F., and T. Lufkin, 2006 Dlx5 and Dlx6 homeobox genes are required for specification of the mammalian vestibular apparatus. Genesis 44: 425–437.
Robledo, R. F., L. Rajan, X. Li, and T. Lufkin, 2002 The Dlx5 and Dlx6 homeobox genes are essential for craniofacial, axial, and appendicular skeletal development. Genes Dev. 16: 1089–1101.
Saheki, T., and K. Kobayashi, 2002 Mitochondrial aspartate glutamate carrier (citrin) deficiency as the cause of adult-onset type II citrullinemia (CTLN2) and idiopathic neonatal hepatitis (NICCD). J. Hum. Genet. 47: 333–341.
Saitsu, H., K. Kurosawa, H. Kawara, M. Eguchi, T. Mizuguchi *et al.*, 2009 Characterization of the complex 7q21.3 rearrangement in a patient with bilateral split-foot malformation and hearing loss. Am. J. Med. Genet. A. 149A: 1224–1230.
Scherer, S. W., P. Poorkaj, T. Allen, J. Kim, D. Geshuri *et al.*, 1994 Fine mapping of the autosomal dominant split hand/split foot locus on chromosome 7, band q21.3-q22.1. Am. J. Hum. Genet. 55: 12–20.
Self, T., M. Mahony, J. Fleming, J. Walsh, S. D. Brown *et al.*, 1998 Shaker-1 mutations reveal roles for myosin VIIA in both development and function of cochlear hair cells. Development 125: 557–566.
Shamseldin, H. E., M. A. Faden, W. Alashram, and F. S. Alkuraya, 2012 Identification of a novel DLX5 mutation in a family with autosomal recessive split hand and foot malformation. J. Med. Genet. 49: 16–20.
Shlyueva, D., G. Stampfel, and A. Stark, 2014 Transcriptional enhancers: from properties to genome-wide predictions. Nat. Rev. Genet. 15: 272–286.
Sinasac, D. S., M. A. Crackower, J. R. Lee, K. Kobayashi, T. Saheki *et al.*, 1999 Genomic structure of the adult-onset type II citrullinemia gene, SLC25A13, and cloning and expression of its mouse homologue. Genomics 62: 289–292.
Sinasac, D. S., M. Moriyama, M. A. Jalil, L. Begum, M. X. Li *et al.*, 2004 Slc25a13-knockout mice harbor metabolic deficits but fail to display hallmarks of adult-onset type II citrullinemia. Mol. Cell. Biol. 24: 527–536.
Sowinska-Seidler, A., M. Badura-Stronka, A. Latos-Bielenska, M. Stronka, and A. Jamsheer, 2014 Heterozygous DLX5 nonsense mutation associated with isolated split-hand/foot malformation with reduced penetrance and variable expressivity in two unrelated families. Birth Defects Res. A Clin. Mol. Teratol. 100: 764–771.
Spitz, F., and D. Duboule, 2008 Global control regions and regulatory landscapes in vertebrate development and evolution. Adv. Genet. 61: 175–205.
Spitz, F., F. Gonzalez, and D. Duboule, 2003 A global control region defines a chromosomal regulatory landscape containing the HoxD cluster. Cell 113: 405–417.
Tackels-Horne, D., A. Toburen, E. Sangiorgi, F. Gurrieri, X. de Mollerat *et al.*, 2001 Split hand/split foot malformation with hearing loss: first report of families linked to the SHFM1 locus in 7q21. Clin. Genet. 59: 28–36.
Tayebi, N., A. Jamsheer, R. Flottmann, A. Sowinska-Seidler, S. C. Doelken *et al.*, 2014 Deletions of exons with regulatory activity at the DYNC1I1 locus are associated with split-hand/split-foot malformation: array CGH screening of 134 unrelated families. Orphanet J. Rare Dis. 9: 108.

Tian, C., L. H. Gagnon, C. Longo-Guess, R. Korstanje, S. M. Sheehan *et al.*, 2017 Hearing loss without overt metabolic acidosis in ATP6V1B1 deficient MRL mice, a new genetic model for non-syndromic deafness with enlarged vestibular aqueducts. Hum. Mol. Genet. 26: 3722–3735.

Truett, G. E., P. Heeger, R. L. Mynatt, A. A. Truett, J. A. Walker *et al.*, 2000 Preparation of PCR-quality mouse genomic DNA with hot sodium hydroxide and tris (HotSHOT). Biotechniques 29: 52, 54.

van Silfhout, A. T., P. C. van den Akker, T. Dijkhuizen, J. B. Verheij, M. J. Olderode-Berends *et al.*, 2009 Split hand/foot malformation due to chromosome 7q aberrations(SHFM1): additional support for functional haploinsufficiency as the causative mechanism. Eur. J. Hum. Genet. 17: 1432–1438.

Visel, A., S. Minovitsky, I. Dubchak, and L. A. Pennacchio, 2007 VISTA Enhancer Browser–a database of tissue-specific human enhancers. Nucleic Acids Res. 35: D88–D92.

Visel, A., E. M. Rubin, and L. A. Pennacchio, 2009 Genomic views of distant-acting enhancers. Nature 461: 199–205.

Wang, X., Q. Xin, L. Li, J. Li, C. Zhang *et al.*, 2014 Exome sequencing reveals a heterozygous DLX5 mutation in a Chinese family with autosomal-dominant split-hand/foot malformation. Eur. J. Hum. Genet. 22: 1105–1110.

Warming, S., N. Costantino, D. L. Court, N. A. Jenkins, and N. G. Copeland, 2005 Simple and highly efficient BAC recombineering using galK selection. Nucleic Acids Res. 33: e36.

Wieland, I., P. Muschke, S. Jakubiczka, M. Volleth, B. Freigang *et al.*, 2004 Refinement of the deletion in 7q21.3 associated with split hand/foot malformation type 1 and Mondini dysplasia. J. Med. Genet. 41: e54.

Zuniga, A., O. Michos, F. Spitz, A. P. Haramis, L. Panman *et al.*, 2004 Mouse limb deformity mutations disrupt a global control region within the large regulatory landscape required for Gremlin expression. Genes Dev. 18: 1553–1564.

Communicating editor: T. Magnuson